THE JOURNAL OF PROSTHETIC DENTISTRY

RESEARCH AND EDUCATION

Effect of 1.5-T and 3.0-T magnetic resonance imaging on the ceramic adhesion and physical properties of prosthetic substructures

Nurten Baysal, PhD,[a] Simel Ayyıldız, PhD, DDS,[b] Ilghar Orujalipoor, PhD,[c] and Barış Filiz Erol, PhD[d]

ABSTRACT

Statement of problem. Magnetic resonance imaging (MRI) is a cross-sectional imaging technique that is widely used in the detection of pathologies in the head and neck region. However, information is lacking about the effect of MRI imaging on the clinical success of fixed partial dentures (FPDs).

Purpose. The purpose of this in vitro study was to analyze the effect of MRI on the physical properties and ceramic adhesion of FPD substructure materials.

Material and methods. Three hundred disk (12×1 mm) and 255 rectangular (4×2×2 mm) specimens were prepared with different fabrication techniques for 5 experimental groups: direct metal laser sintering (DMLS) with Co-Cr and Ti; casting with Co-Cr and Ni-Cr; and milling with ZrO_2. After ceramic application, the disk specimens were subjected to aging and divided into 3 subgroups (n=20) with exposure to 1.5-T and 3.0-T MRI brain scans for 30 minutes and no exposure (control). The shear bond strength (SBS) of the specimens was measured by using a universal testing machine. The rectangular specimens were exposed to MRI with the same procedure, and the nanostructure of the specimens was analyzed with the small-angle X-ray scattering (SAXS) method to detect the nanoscale structural effects of MRI. The average surface roughness (Ra) and Vickers microhardness (Vh) were also measured for complementary analyses. SBS, Ra, and Vh values were statistically analyzed by 1-way ANOVA and the Tukey honestly significant difference test (α=.05).

Results. The SBS (MPa) of casting groups (P<.001) and DMLS with the Co-Cr group (P<.05) were significantly affected by MRI exposures. The significant differences were seen on the Ra of casting (P<.001) and DMLS with Co-Cr (P<.05) and Ti (P<.01) groups. Also, the Vh of the casting with Co-Cr (P<.001) and Ni-Cr (P<.01) groups showed significant differences. The SAXS analysis indicated that the physical properties of materials were influenced by MRI exposure.

Conclusions. The results indicated that MRI applications affected the metal-ceramic adhesion of Co-Cr and Ni-Cr dental alloys produced by casting and the DMLS technique. (J Prosthet Dent 2020;■:■-■)

Metal-ceramic restorations have been popular because of their long-term clinical success,[1-6] although base metal alloys such as Co-Cr, Ni-Cr, and Ti have replaced precious alloys.[2,3,7] Co-Cr alloys are the most popular because of their high biocompatibility, high corrosion resistance, and low allergenicity.[3,5,6] Ti is an attractive metal for dentistry because of its low density, high durability, high corrosion resistance, and excellent biocompatibility.[8-10] If metal-ceramic restorations cannot meet the esthetic requirements, ceramic systems, particularly zirconia and lithium disilicate, are alternatives.[4,11]

For fixed partial dentures (FPDs), adequate bonding between the substructure and veneering ceramic is essential and is achieved by micromechanical forces and chemical bonding.[1,2,5,12] Various manufacturing techniques have been developed to improve the bond.[13] However, failures of the metal-ceramic bond including incompatibility of the coefficient of thermal expansion between the substructure and veneer ceramics, incomplete wetting of the veneer ceramic to the

Scientific Research Commission of Gulhane Military Medical Academy as grant sponsor The study is funded by Scientific Research Commission of Gulhane Military Medical Academy.
[a]Assistant Professor, Department of Prosthodontics, Faculty of Gulhane Dentistry, University of Health Sciences Turkey, Ankara, Turkey.
[b]Professor, Department of Prosthodontics, Faculty of Gulhane Dentistry, University of Health Sciences Turkey, Ankara, Turkey.
[c]Assistant Professor, Department of Nanotechnology and Nanomedicine, Institute of Science, Hacettepe University, Beytepe, Ankara and Alptek Engineering and Technological Systems AS, Umraniye, 34774, Istanbul Turkey.
[d]Assistant Professor, Department of Prosthodontics, Faculty of Gulhane Dentistry, University of Health Sciences Turkey, Ankara, Turkey.

Clinical Implications

MRI applications may affect the metal-ceramic adhesion and nanostructure of dental alloys with ferromagnetic properties, depending on the strength of the magnetic field.

substructure, improperly designed substructures, and inappropriate firing conditions have been reported.[4,5,11] Also, the magnetic field and nonionized radio waves from magnetic resonance imaging (MRI) application have led to bonding failures.[2]

MRI is a cross-sectional imaging method that allows imaging on different planes without radiation.[14-17] This imaging technique is widely used in the detection of head and neck pathologies, neurological disorders, ophthalmic and pediatric diseases, and brain tumors.[14-17] The energy used by MRI is radio waves, and a strong and uniform static magnetic field is formed.[14-17] MRI devices work with the created magnetic fields in the range of 0.2-7.0 T. The earth's magnetic field is in the range of 0.25 to 0.65 gauss (G) (average 0.5 G) at its surface (1 T=10 000 G). Therefore, a magnetic field of about 20 000 times bigger than that of the earth's magnetic field is used in an MRI device,[16,17] which may affect dental materials.[2,14,17,18] Materials behave in 1 of 3 ways, depending on their sensitivity to the magnetic field. Materials that do not exhibit magnetism in the magnetic field are diamagnetic; substances with unpaired electrons are paramagnetic and become demagnetized when the effect of the magnetic field disappears; substances that are strongly attracted by the magnetic field are ferromagnetic. Iron (Fe), nickel (Ni), and cobalt (Co) are ferromagnetic materials in dental alloys; titanium (Ti) and zirconium (Zr) have paramagnetic properties.[1,2,14,16,17] Dental materials with magnetic properties lead to unfavorable effects such as artifact formation,[17-20] heat generation,[14,15,21] and mechanical displacement.[17] Therefore, the MRI technique has drawbacks for patients with metal dental restorations, orthodontic appliances, and implants.[2,14,15,17-22]

In the present study, the effect of 1.5-T and 3.0-T MRI applications was investigated on the bond strength of ceramic to cast Co-Cr, direct metal laser sintered (DMLS) Co-Cr, cast Ni-Cr, DMLS Ti, and milled zirconia substructures, and changes in the physical properties of the materials were also examined. The null hypothesis was that the physical properties of the materials and metal-ceramic bond would not be affected by exposure to the magnetic field and the nonionized radiofrequency waves of MRI applications.

MATERIAL AND METHODS

The main groups and materials used in the present study are listed in Table 1. Three hundred disk specimens (r=12 mm, h=1 mm) were prepared for 15 experimental groups (n=20) to analyze the shear bond strength (SBS). Additionally, 255 rectangular specimens (4×2×2 mm) were prepared for 15 experimental groups (n=15) to analyze nanostructure. The specimens in this group were produced in a size suitable for the small-angle X-ray scattering (SAXS) device.

To produce casting disk specimens in a standard dimension, a 2-piece aluminum mold was designed (Fig. 1) to produce wax patterns (Cavex Set Up Regular; Cavex), which were invested (Bellavest SH; Bego) and cast by using an induction casting machine (Fornax; Bego) from Ni-Cr (Remanium CSe; Dentaurum) and Co-Cr (Remanium star; Dentaurum) alloys according to the manufacturers' instructions. A mold (Fig. 2) was also designed and used to prepare rectangular specimens. A liquid silicone (Platsil 73-29; Polytek Development Corp) was used to obtain a mold with negative spaces to prepare casting wax patterns (Kronenwachs; Bego). The Ni-Cr and Co-Cr rectangular specimens were cast by using the same procedure as the disk specimens.

In the DMLS groups, the shape of the 3D specimens was digitized with a design software program (DWOS software; Dental Wings Inc, 2018). First, Co-Cr (Remanium star CL; Dentaurum) and then Ti powders (Cl41TiEli; GE Additive Co) were laser sintered by means of a laser metal sintering machine (M2 Cusing; Concept Laser GmbH) according to the digital design (200 W ytterbium (Yb)-fiber optical laser, scanning speed of 7 m/s, and layer thickness of 30 μm). The specimens were annealed in a furnace (XD 1600A; Zhengzhou Brother Furnace Co) in an argon atmosphere (temperature range of Co-Cr alloy: 300 °C to 1150 °C and Ti alloy: 500 °C to 840 °C).

To prepare zirconia specimens from semisintered yttrium stabilized ZrO_2 blocks (Nacera Pearl; Doceram) on a computer numerical control (CNC) milling machine (Yenadent D43; Yenadent), the same 3D program was used. The specimens were sintered at 1500 °C in a furnace (Tegra MP1500; Teknik Dental).

After the fabrication process, 1 surface of the rectangular specimens was finished with 300- and 600-grit abrasive paper (Water Proof Paper; Atlas English Abrasives). All rectangular and disk specimens were then airborne-particle abraded with110-μm Al_2O_3 particles (Korax; Bego) under 0.5-MPa air pressure for 10 seconds at a 2-cm distance, steam cleaned, and ultrasonically cleaned in distilled water for 5 minutes. Before ceramic application, the specimens were stored in trichloroethylene solution for 5 seconds to remove the Al_2O_3 particles.

The ceramic was applied to the disk specimens (h=4 mm, r=6 mm) by using custom-made molds (Figs. 3), according to the manufacturer's instructions. Ceramics that were used for each group are shown in Table 2. To standardize the dimension of the ceramic, the disk

Table 1. Group names, manufacturer, composition, and fabrication process of materials used. C; cast, L; laser, M; milled

Material	Manufacturer	Composition	Process
Co-Cr_C	Remanium star; Dentaurum	Co 60.5%, Cr 28%, W 9%, Si 1.5%, others: <1%: Mn, N, Nb	Lost-wax casting
Co-Cr_L	Remanium star CL; Dentaurum	Co 60.5%, Cr 28%, W 9%, Si 1.5%, others: <1%: Mn, N, Nb, Fe	Direct metal laser sintering
Ni-Cr_C	Remanium CSe; Dentaurum	Ni 61%, Cr 26%, Mo 11%, Si 1.5%, others: <1% Co, Fe, Al, Ce	Lost-wax casting
Ti_L (grade 23)	CL41TIELI; GE Additive Company	Ti 90%, Al 5.5-6.5%, V 3.5-4.5%, Fe 0.25%, C 0.08%, N 0.05%, O 0.13%, H 0.012%	Direct metal laser sintering
ZrO_2_M	Nacera Pearl; Doceram	ZrO_2, Y_2O_3, HfO_2, Al_2O_3	CAD-CAM milling

C, cast; L, laser; M, milled.

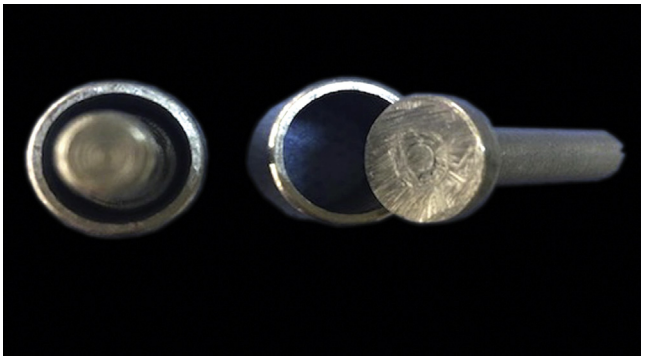

Figure 1. Aluminum molds for disk specimens.

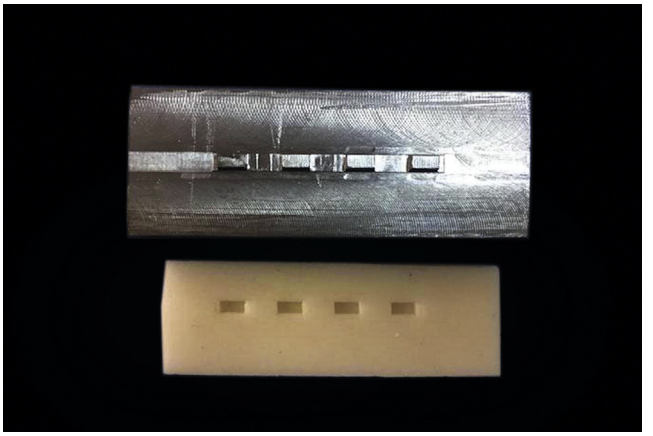

Figure 2. Aluminum and silicone molds for rectangular specimens.

specimens were placed on a gypsum cast and ground by using a fine grain diamond rotary instrument (SRD 07; Syndent Tools Co) at 15 000 rpm with the handpiece in a parallelometer (AF350; Amann Girrbach AG). Thickness was measured by using digital calipers (Digital ABS AOS Caliper; Mitutoyo Corp). The specimens were subjected to an aging procedure consisting of exposure to ultraviolet (UV) light and water spray in a weathering machine (Xenotest 150 S+; Atlas Material Testing Technology) for 200 hours. The temperature of the weathering machine varied between 70 °C (light) and 38 °C (dark), and a humidity of between 50% (light) and 95% (dark). The testing cycle consisted of 40 minutes of light only, 20 minutes of light with front water spray, 60 minutes of light only, and 60 minutes of dark with back water spray (66 cycles). In the weathering machine, the dry bulb temperature of the air was 38 °C (dark), and 47 °C (light), and the water temperature was 50 °C.

To see the effect of MRI, the disk specimens of 5 different study groups were assigned to 3 subgroups, exposed 30 minutes to 1.5 T (Philips Achieva 1.5-T X-Series; Royal Philips Electronics), exposed 30 minutes to 3.0 T (Philips Achieva 3.0-T X-Series; Royal Philips Electronics), and the control unexposed to MRI. The specimens were put in sterile plastic cups filled with saline solution (Isolyte 1000 mL; Eczacıbaşı-Baxter), and the cups were placed in a larger plastic container. By using a standard head and neck coil, the plastic containers were placed on the bench of the1.5-T and 3.0-T MRI devices. The brain MRI sequences were applied to the specimens, which were scanned with T2-weighted (T2W) turbo spin echo (TSE) in the axial and coronal planes and T1W inversion recovery (IR) TSE-based sequencing in the axial plane. The radiofrequency (RF) power output gain was adjusted manually. The exposure to the MRI was in the following sequence: T2W-axial, T2W-flair axial, T1-axial, diffusion, T2W-coronal, T1-3D-sagittal.[14,15,18]

For the shear test, the disk specimens were embedded in autopolymerizing acrylic resin (Panacryl; İnci Dental) by using plastic molds (15×15×15 mm). Shear force was applied to the metal-ceramic interface in a universal testing machine (LRX Plus; Lloyd Instruments) with a shearing blade at a crosshead speed of 1 mm/min. Peak force values (N) at failure were recorded and divided by the surface area to obtain the bond strength values (MPa).

Rectangular specimens of each alloy type were divided into 3 subgroups. After MRI exposure, 5 specimens were selected from each group, and average surface roughness (Ra) was determined by using a contact profilometer (TR100 Surface Roughness Tester; Checkline Europe BV) over evaluation lengths of 4 mm and cutoff value as 0.25 mm from 3 readings per group (measuring range Ra: 0.05 to 15.0 μm).

The microhardness of 5 specimens from each group was measured, and 3 measurements were performed per group by using a digital Vickers microhardness (Vh)

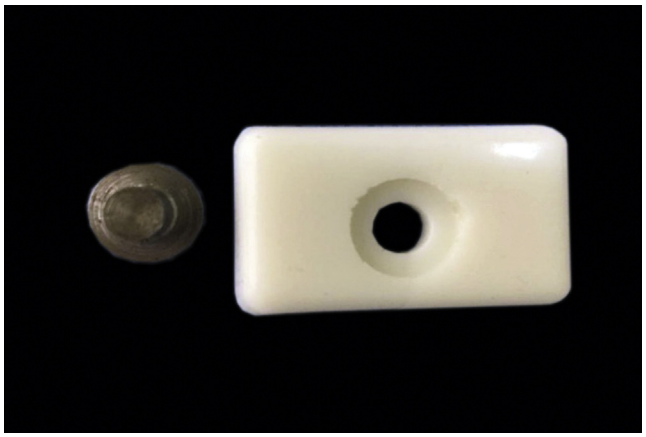

Figure 3. Silicone and metal molds for application of ceramic.

tester (Model FM-7; Future Tech). The measurement was carried out with a diamond pyramid tip with a square cross-section and at a peak angle of 136 degrees with 9.8 N per 5 seconds. An additional 5 rectangular specimens from each group were selected for analysis with the HECUS SAXS system3 (Hecus X-ray systems; Bruker Austria GmbH) method to detect nanoscale structural effects from exposure to MRI.[7]

Statistical analysis was performed by using a software program (R version 3.6.1/2019; R Foundation). The results of the SBS, Ra, and Vh were statistically analyzed with 1-way ANOVA and the Tukey honestly significant difference (HSD) test (α=.05)

RESULTS

The results of the 1-way ANOVA test for estimating the effect of 1.5-T and 3.0-T MRI application on the SBS, Ra, and Vh of the experimental groups are summarized in Table 3. The descriptive statistics and mean values of SBS, Ra, and Vh are shown in Table 4.

According to the Tukey HSD test results (Table 4), the SBS of the Co-Cr_Ca and Ni-Cr_Cb groups increased and that of the Co-Cr_Cb and Ni-Cr_Ca groups decreased significantly compared with their control groups (P<.001). Additionally, the Co-Cr_La group showed a higher bond strength value than the Co-Cr_Lb group (P<.05). The Ra of the Co-Cr_Cb (P<.001) and Ti_La (P=.005) groups increased while it decreased for the Co-Cr_La (P=.023) group with respect to their control groups. The Vh values of the casting groups showed significant differences. The Vh of the Co-Cr_Cb group decreased compared with that of the Co-Cr_Cc and Co-Cr_Ca groups (P<.001) and that of the Ni-Cr_Cb group increased compared with that of the Ni-Cr_Cc and Ni-Cr_Ca groups (P<.01). No significant differences were seen in the ZrO_2_M group (P>.05).

Figure 4 demonstrates the SAXS results of the Co-Cr_C, Ni-Cr_C, and Co-Cr_L groups. A, D, and G present the small angle data (q=scattering vector) of the experimental groups. The scattering patterns of the specimens provided information about the overall size and shape of their nanostructure. The pair distance distributions (PDDs) (Fig. 4B, 4E, 4H) provided information about the distances between particles, and the data from these analyses provided information about the homogeneity of the material examined. The scattering data in the SAXS analyses were obtained from electrons in the structure of the matter examined. The radial electron densities (rho(r)) (Fig. 4C, 4F, 4I) provided information about the electron densities of the experimental groups.

Table 2. Ceramic materials for specimen groups used

Specimen Groups	Ceramic Materials
Co-Cr_C, Co-Cr_L, Ni-Cr_C	Ceramco 3 Dentin; Dentsply Sirona
Ti_L	Super Porcelain TI-22; Noritake Dental Supply Co
ZrO_2_M	Ceramco PFZ Dentin; Dentsply Sirona

DISCUSSION

Based on the findings, the null hypothesis that the physical properties of the materials and metal-ceramic bond would not be affected by exposure to the magnetic field and nonionized radiofrequency waves of MRI applications was rejected for Co-Cr_C, Ni-Cr_C, and Co-Cr_L specimens. The ZrO_2 _M and Ti-L were not affected significantly except for the Ra of Ti_L.

Several factors, including the oxide layer thickness of the metal,[5,8-10,12] production technique of the framework material,[13] alloy type,[23] aging,[6,11] mechanical loading applications,[6,10] and MRI applications,[2] have been reported to influence bond strength. In the present study, a 1-week aging process that corresponded to 1 year of clinical use was performed. Then, 30 minutes of MR brain imaging sequences were exposed with 1.5-T and 3.0-T MRI devices. As a result of these applications, the SBS of the Co-Cr_Ca and Ni-Cr_Cb groups showed an increase, whereas the Co-Cr_Cb, Ni-Cr_Ca, and Co-Cr_Lb groups showed a decrease compared with the control groups. Co-Cr and Ni-Cr are MRI-incompatible[18,22] alloys, and the differences in SBS are considered to be from changes in the metal-ceramic interfaces and physical properties of the specimens.

El-Bediwi et al[2] reported that the Ra of Ti and Ni-Cr alloys increased after MRI exposure. In the present study, the Ra of the Ti_La and Co-Cr_Cb groups increased and that of the Co-Cr-La group decreased compared with the control groups. The differences in magnetic field strength could affect the materials in different ways, which is supported by the results of the SAXS analysis. The rho(r) images of the SAXS analysis show that differences were found in the electron densities of specimens after MRI application (Fig. 4C, 4F, 4I), probably from differences in radial electron densities.

Table 3. One-way ANOVA results for shear bond strength (MPa), Vickers microhardness (Vh), and surface roughness (Ra) of specimen groups

Experimental Treatments	Source of Variation	*df*	SS	MS	F	*P*
Shear bond strength (SBS)			—			
Group 1 Co-Cr_C	Between groups	2	214.8	107.4	60.7	<.001
	Within groups	57	100.8	1.7	—	—
Group 2 Co-Cr_L	Between groups	2	29.9	14.9	3.7	.029
	Within groups	57	228.1	4.0	—	—
Group 3 Ni-Cr_C	Between groups	2	1016.9	508.4	81.2	<.001
	Within groups	57	356.7	6.2	—	—
Group 4 Ti_L	Between groups	2	39.3	19.6	2.5	.090
	Within groups	57	447.1	7.8	—	—
Group 5 Zr_M	Between groups	2	3.1	1.5	0.1	.850
	Within groups	57	548.8	9.6	—	—
Surface roughness (Ra)			—			
Group 1 Co-Cr_C	Between groups	2	0.7	0.3	16.2	<.001
	Within groups	12	0.2	0.0	—	—
Group 2 Co-Cr_L	Between groups	2	0.3	0.1	4.8	.028
	Within groups	12	0.3	0.0	—	—
Group 3 Ni-Cr_C	Between groups	2	0.0	0.0	0.2	.805
	Within groups	12	0.5	0.0	—	—
Group 4 Ti_L	Between groups	2	0.7	0.3	7.7	.006
	Within groups	12	0.6	0.0	—	—
Group 5 Zr_M	Between groups	2	0.0	0.0	0.0	.998
	Within groups	12	0.3	0.0	—	—
Vickers microhardness (Vh)			—			
Group 1 Co-Cr_C	Between groups	2	45 026.8	22 513.4	17.3	<.001
	Within groups	12	15 537.6	1294.8	—	—
Group 2 Co-Cr_L	Between groups	2	217.2	108.6	0.2	.750
	Within groups	12	4441.2	370.1	—	—
Group 3 Ni-Cr_C	Between groups	2	17 889.7	8944.8	9.8	.002
	Within groups	12	10 852	904.3	—	—
Group 4 Ti_L	Between groups	2	200.1	100.0	0.3	.686
	Within groups	12	3097.6	258.1	—	—
Group 5 Zr_M	Between groups	2	2078.4	1039.2	0.1	.840
	Within groups	12	70 621.2	5885.1	—	—

Hardness is defined as the resistance of the material surface to permanent shape change[1,3] and is affected by heat,[7] which is increased during MRI exposure.[14,15,17,21,22] El-Bediwi et al[2] reported that MRI applications lead to a decrease in the Vh values of pure Ti cast and Ni-Cr alloys and stated that this decrease might be caused by heat increase. However, others have reported that the heat increase of dental materials was minimal (between 0.6 °C and 1.80 °C) after MRI applications.[14,15,21,22] Therefore, it is unlikely these small heat changes affect the hardness of the dental metals. Only very high (such as 800 °C for Co-Cr) heat changes have been reported to influence the hardness of dental metals.[24] Therefore, the differences in the hardness of the alloys are probably a result of the magnetic fields and nonionized radio waves of MRI applications changing the nanostructure.

Table 4. Descriptive statistics for SBS (MPa), surface roughness (Ra), and Vickers microhardness (Vh) of experimental groups

Test	Grouping	N	Mean ±SD	Minimum	Maximum
SBS	Co-Cr_Ca[b,c]	20	24.1 ±1.2	21.3	25.7
	Co-Cr_Cb[a,c]	20	19.4 ±0.9	17.5	20.8
	Co-Cr_Cc[a,b]	20	21.7 ±1.6	18.0	23.9
	Co-Cr_La[b]	20	20.4 ±2.5	13.8	26.3
	Co-Cr_Lb[a]	20	18.8 ±1.4	15.6	20.9
	Co-Cr_Lc	20	19.0 ±1.7	16.6	22.9
	Ni-Cr_Ca[b,c]	20	18.1 ±2.5	14.6	24.5
	Ni-Cr_Cb[a,c]	20	28.0 ±2.1	24.0	31.2
	Ni-Cr_Cc[a,b]	20	21.2 ±2.7	18.6	28.3
	Ti_La	20	19.7 ±3.0	13.0	25.2
	Ti_Lb	20	17.9 ±2.2	14.2	22.4
	Ti_Lc	20	19.4 ±3.0	12.4	23.9
	Zr_Ma	20	16.7 ±2.9	11.1	19.7
	Zr_Mb	20	16.3 ±2.5	12.3	23.1
	Zr_Mc	20	16.2 ±3.7	11.2	22.4
Ra	Co-Cr_Ca[b]	5	1.9 ±0.1	1.8	2.1
	Co-Cr_Cb[a,c]	5	2.3 ±0.1	2.1	2.4
	Co-Cr_Cc[a]	5	1.7 ±0.2	1.5	2.0
	Co-Cr_La[c]	5	1.1 ±0.1	1.0	1.4
	Co-Cr_Lb	5	1.3 ±0.2	1.2	1.7
	Co-Cr_Lc[a]	5	1.5 ±0.1	1.4	1.6
	Ni-Cr_Ca	5	1.5 ±0.2	1.1	1.7
	Ni-Cr_Cb	5	1.6 ±0.1	1.3	1.7
	Ni-Cr_Cc	5	1.6 ±0.2	1.4	1.8
	Ti_La[c]	5	1.3 ±0.2	1.0	1.6
	Ti_Lb	5	1.0 ±0.2	0.8	1.3
	Ti_Lc[a]	5	0.7 ±0.2	0.4	1.0
	Zr_Ma	5	0.3 ±0.1	0.2	0.5
	Zr_Mb	5	0.3 ±0.1	0.1	0.5
	Zr_Mc	5	0.3 ±0.1	0.1	0.6
Vh	Co-Cr_Ca[b]	5	458.6 ±39.2	426	520
	Co-Cr_Cb[a,c]	5	333.6 ±34.3	304	381
	Co-Cr_Cc[b]	5	438.4 ±34.1	399	481
	Co-Cr_La	5	509.6 ±13.0	495	527
	Co-Cr_Lb	5	500.6 ±22.4	477	533
	Co-Cr_Lc	5	507.2 ±20.9	482	525
	Ni-Cr_Ca[a]	5	310.8 ±41.7	269	366
	Ni-Cr_Cb[a,c]	5	391 ±16.0	375	409
	Ni-Cr_Cc[b]	5	327.6 ±26.6	284	354
	Ti_La	5	401.8 ±19.3	383	433
	Ti_Lb	5	393 ±7.1	383	399
	Ti_Lc	5	398.8 ±18.6	377	425
	Zr_Ma	5	1504.6 ±83.9	1388	1609
	Zr_Mb	5	1491.4 ±75.3	1402	1583
	Zr_Mc	5	1520.2 ±70.2	1468	1643

Different superscript letters represent significant differences ($P<.05$) among groups. Subgroup names a, 30 minutes 1.5-T; b, 30 minutes 3.0-T; c, control; SD, standard deviation.

Co-Cr_C, Ni-Cr_C, and Co-Cr_L specimens showed differences in their SAXS profiles, PDDs, and rho(r) (Fig. 4). The hardness of the alloys can be explained with the peak intensity value (Å) of the hump-shaped distance in PDDs (Fig. 4B, 4E, 4H). According to the control group's

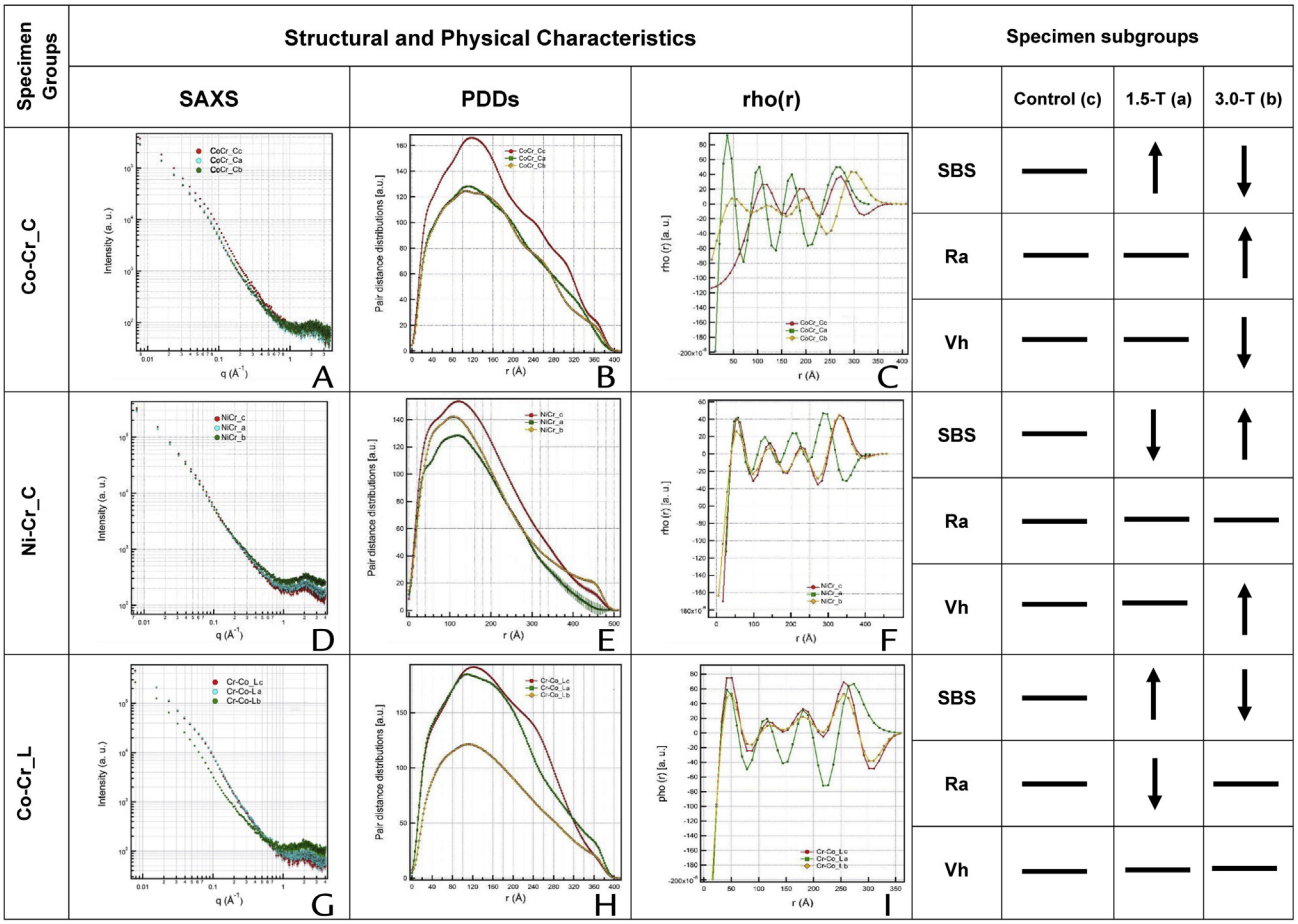

Figure 4. SAXS profiles: I (q)-q data. I, scattered intensity; PDDs, pair distance distributions show distances of nano-aggregations; q, scattering vector; Ra, surface roughness; rho(r)-r, radial electron densities; SAXS, small-angle x-ray scattering; SBS, shear bond strength; Vh, Vickers hardness.

nanoformations, the effect of magnetic field on 3D nanoglobular aggregations has appeared as shape differences. The shape changed from spherical forms to the more cylindrical morphologies as expected. For the Co-Cr_C group, the most possible distance values between the nanoglobules were equal to 118.9 Å (Co-Cr_Cc), 112.7 Å (Co-Cr_Ca), and 125.0 Å (Co-Cr_Cb). The decrease in PDD value indicated that the interactions between the nanoglobules of the Co-Cr_Ca group increased and that this led to the increase in the Vh of the Co-Cr_Ca (458.6 ±39.2 HV1) group. The increase in PDD value of the Co-Cr_Cb group indicated that the interaction between nanoglobules decreased, so the Vh of this group (333.6 ±34.3 HV1) also decreased. The most possible distance values between the nanoglobules of the Ni-Cr_C group were equal to 120.3 Å (Ni-Cr_Cc), 121.7 Å (Ni-Cr_Ca), and 112.1 Å (Ni-Cr_Cb). From these values, the increase in the Vh of the Ni-Cr_Cb (391 ±16.0 HV1) group compared with that of the Ni-Cr_Cc (327.6 ±26.6 HV1) and Ni-Cr_Ca (310.8 ±41.7 HV1) groups can be explained by the increase in interaction between nanoglobules. The Vh values of the Co-Cr_L group were not as affected by the MRI application as the casting groups, probably a result of the different production techniques. The DMLS technique decreased the interparticle thickness and bilayer thickness of the material and eliminated defects and production errors.[7,14]

Ni and Co are ferromagnetic metals,[1,17] so their magnetic dipole moments can change directions from the effect of an external magnetic field, affecting mechanical properties. Co has a hexagonal crystallization form, and Ni is cubic.[1] Alloys made with these metals form rod-shaped nanocrystals (Co) or globular or cylinder close to globular (Ni).[1,25] With the addition of Cr in this structure, variations in these shapes may occur, and the hardness may also increase or decrease depending on the variations in the magnetic dipole orientations. The increase in Ni-Cr hardness in a 3.0-T magnetic field may be an indication that magnetic dipoles and globular ferromagnetic grains are oriented in parallel directions. Additionally, the formation of intersite physicochemical bonds and particle distances affected the mechanical properties of the material.[26] The regions and clusters associated with nanoparticles also directly affect the

mechanical properties of metal alloys.[1,3,26] The changes in the production stages of metals also cause differences in the physical properties of the materials.[1,3,26] In future studies, these findings can be evaluated by scanning electron microscopy (SEM) and energy dispersion x-ray spectrum (EDS) analyses, which allow for a more detailed examination of the surfaces.

Considering the changes in nanostructural, physical, and metal-ceramic bonding of the materials after MRI applications, paramagnetic materials could be recommended to protect the fixed partial restorations from MRI signals. However, this aspect needs to be verified with clinical studies.

CONCLUSIONS

Based on the findings of this in vitro study, the following conclusions were drawn:

1. A 30-minute 1.5-T MRI application decreased the metal-ceramic bond of Ni-Cr alloy but increased the bond of cast and DMLS Co-Cr alloys. A 30-minute 3.0-T MRI application increased the metal-ceramic bond of Ni-Cr alloy while decreasing the bond of cast and DMLS Co-Cr alloys.
2. A 30-minute 1.5-T MRI application increased the surface roughness of DMLS Ti but decreased the roughness of DMLS Co-Cr alloy. A 30-minute 3.0-T MRI application increased the surface roughness of casting with Co-Cr alloy.
3. A 30-minute 3.0-T MRI application decreased the Vickers microhardness of casting with Co-Cr alloy but increased the microhardness of Ni-Cr alloy.
4. The MRI applications led to significant effects on the metal-ceramic bond and physical properties of ferromagnetic substructure materials used in fixed partial dentures as seen in SAXS profiles, PDDs, and rho(r).

REFERENCES

1. Anusavice KJ, Shen C, Rawls HR. Phillip's science of dental materials. 12th ed. St. Louis: Mosby/Elsevier; 2012. p. 48-92.
2. El-Bediwi AB, El-Fallal A, Saker S, Özcan M. Effect of non-ionizing radio frequency signals of magnetic resonance imaging on physical properties of dental alloys and metal-ceramic adhesion. J Adhes Dent 2014;16:407-13.
3. Henriques B, Soares D, Silva FS. Microstructure, hardness, corrosion resistance and porcelain shear bond strength comparison between cast and hot pressed Co-CrMo alloy for metal-ceramic dental restorations. J Mech Behav Biomed Mater 2012;12:83-92.
4. Zaher AM, Hochstedler JL, Rueggeberg FA, Kee EL. Shear bond strength of zirconia-based ceramics veneered with 2 different techniques. J Prosthet Dent 2017;118:221-7.
5. Sipahi C, Özcan M. Interfacial shear bond strength between different base metal alloys and five low fusing feldspathic ceramic systems. Dent Mater J 2012;31:333-7.
6. Trindade FZ, Anami LC, da Costa Lima JM, Oliveira de Vasconcellos LG, Balducci I, Nogueira Júnior L, et al. The effect of a bonding agent and thermo-mechanical cycling on the bond strength of a glass-ceramic to gold and cobalt-chromium alloys. Appl Adhes Sci 2014;2:16.
7. Ayyıldız S, Soylu EH, Ide S, Kılıç S, Sipahi C, Pişkin B, et al. Annealing of Co-Cr dental alloy: effects on nanostructure and Rockwell hardness. J Adv Prosthodont 2013;5:471-8.
8. Toptan F, Alves AC, Henriques B, Souza JC, Coelho R, Silva FS, et al. Influence of the processing route of porcelain/Ti-6Al-4V interfaces on shear bond strength. J Mech Behav Biomed Mater 2013;20:327-37.
9. Zhang CC, Ye JT, Zhang YP, Liao JK, Li BH. Effect of titanium preoxidation on wrought pure titanium to ceramic bond strength. J Prosthet Dent 2013;109:106-12.
10. Vásquez VZC, Özcan M, Kimpara ET. Evaluation of interface characterization and adhesion of glass ceramics to commercially pure titanium and gold alloy after thermal- and mechanical-loading. Dent Mater 2009;25:221-31.
11. Zarone F, Russo S, Sorrentino R. From porcelain-fused-to-metal to zirconia: clinical and experimental considerations. Dent Mater 2011;27:83-96.
12. Enghardt S, Richter G, Richter E, Reitemeier B, Walter M. Experimental investigations on the influence of adhesive oxides on the metal-ceramic bond. Metals (Basel) 2015;5:119-30.
13. Tulga A. Effect of annealing procedure on the bonding of ceramic to cobalt-chromium alloys fabricated by rapid prototyping. J Prosthet Dent 2018;119:643-9.
14. Ayyildiz S, Kamburoğlu K, Sipahi C, Murat S, Görgülü S, Pişkin B. Radiofrequency heating and magnetic field interactions of fixed partial dentures during 3-tesla magnetic resonance imaging. Oral Surg Oral Med Oral Pathol Oral Radiol 2013;116:640-7.
15. Görgülü S, Ayyildiz S, Kamburoğlu K, Gökçe S, Ozen T. Effect of orthodontic brackets and different wires on radiofrequency heating and magnetic field interactions during 3-T MRI. Dentomaxillofacial Radiol 2014;43:20130356.
16. Hashemi RH, Lisanti CJ, Bradley WG. MRI the basics. 4th. ed. Philadelphia: Wolters Kluwer; 2018. p. 1-197.
17. Mathew CA, Maller S, Maheshwaran. Interactions between magnetic resonance imaging and dental material. J Pharm Bioallied Sci 2013;5:113-6.
18. Tymofiyeva O, Vaegler S, Rottner K, Boldt J, Hopfgartner AJ, Proff PC, et al. Influence of dental materials on dental MRI. Dentomaxillofacial Radiol 2013;42.
19. Klinke T, Daboul A, Maron J, Gredes T, Puls R, Jaghsi A, et al. Artifacts in magnetic resonance imaging and computed tomography caused by dental materials. PLoS One 2012;7:1-6.
20. Starčuková J, Starčuk Z, Hubálková H, Linetskiy I. Magnetic susceptibility and electrical conductivity of metallic dental materials and their impact on MR imaging artefacts. Dent Mater 2008;24:715-23.
21. Hasegawa M, Miyata K, Abe Y, Ishigami T. Radiofrequency heating of metallic dental devices during 3.0 T MRI. Dentomaxillofacial Radiol 2013;42:20120234.
22. Miyata K, Hasegawa M, Abe Y, Tabuchi T, Namiki T, Ishigami T. Radiofrequency heating and magnetically induced displacement of dental magnetic attachments during 3.0 T MRI. Dentomaxillofacial Radiol 2012;41:668-74.
23. Joias RM, Tango RN, Junho de Araujo JE, Junho de Araujo MA, Ferreira Anzaloni Saavedra Gde S, Paes-Junior TJ, et al. Shear bond strength of a ceramic to Co-Cr alloys. J Prosthet Dent 2008;99:54-9.
24. Gao M, Alman D. Searching for next single-phase high-entropy alloy compositions. Entropy 2013;15:4504-19.
25. Taylor A. Lattice parameter of binary nickel-cobalt alloys. J Inst Metals 1950;77:585.
26. Casati R, Vedani M. Metal matrix composites reinforced by nano-particles—a review. Metals (Basel) 2014;4:65-83.

Corresponding author:
Dr Nurten Baysal
Department of Prosthodontics
University of Health Sciences Turkey, Faculty of Gulhane Dentistry
Emrah Mah. Gn Tevfik Sağlam Cad, No:1, Etlik, Keçiören, Ankara
TURKEY
Email: nurtenerdogan7@hotmail.com

Acknowledgments
The authors thank Professor Dr Semra İde for helpful discussions and Dr Fatih Erol for his contributions in statistical analyses of this study.

Copyright © 2020 by the Editorial Council for *The Journal of Prosthetic Dentistry*.
https://doi.org/10.1016/j.prosdent.2020.04.027